Atmos. Chem. Phys. Discuss., 13, 12135–12176, 2013
www.atmos-chem-phys-discuss.net/13/12135/2013/
doi:10.5194/acpd-13-12135-2013

Atmospheric Chemistry and Physics Discussions

A sensitivity study of radiative fluxes at the top of atmosphere to cloud-microphysics and aerosol parameters in the Community Atmosphere Model CAM5

C. Zhao[1], X. Liu[1], Y. Qian[1], J. Yoon[1], Z. Hou[1], G. Lin[1], S. McFarlane[1,*], H. Wang[1], B. Yang[2], P.-L. Ma[1], H. Yan[1], and J. Bao[1]

[1]Pacific Northwest National Laboratory, Richland, WA, USA
[2]School of Atmospheric Sciences, Nanjing University, Nanjing, China
[*]now at: Department of Energy, Washington, DC, USA

Received: 11 April 2013 – Accepted: 28 April 2013 – Published: 8 May 2013

Correspondence to: C. Zhao (chun.zhao@pnnl.gov)

Published by Copernicus Publications on behalf of the European Geosciences Union.

Abstract

In this study, we investigated the sensitivity of net radiative fluxes (FNET) at the top of atmosphere (TOA) to 16 selected uncertain parameters mainly related to the cloud microphysics and aerosol schemes in the Community Atmosphere Model version 5 (CAM5). We adopted a quasi-Monte Carlo (QMC) sampling approach to effectively explore the high dimensional parameter space. The output response variables (e.g., FNET) were simulated using CAM5 for each parameter set, and then evaluated using the generalized linear model analysis. In response to the perturbations of these 16 parameters, the CAM5-simulated global annual mean FNET ranges from −9.8 to 3.5 $W m^{-2}$ compared to the CAM5-simulated FNET of 1.9 $W m^{-2}$ with the default parameter values. Variance-based sensitivity analysis was conducted to show the relative contributions of individual parameter perturbation to the global FNET variance. The results indicate that the changes in the global mean FNET are dominated by those of net cloud forcing (CF) within the parameter ranges being investigated. The threshold size parameter related to auto-conversion of cloud ice to snow is identified as one of the most influential parameters for FNET in CAM5 simulations. The strong heterogeneous geographic distribution of FNET variance shows parameters have a clear localized effect over regions where they are acting. However, some parameters also have non-local impacts on FNET variance. Although external factors, such as perturbations of anthropogenic and natural emissions, largely affect FNET variance at the regional scale, their impact is weaker than that of model internal parameters in terms of simulating global mean FNET. The interactions among the 16 selected parameters contribute a relatively small portion to the total FNET variance over most regions of the globe. This study helps us better understand the parameter uncertainties in the CAM5 model, and thus provides information for further calibrating uncertain model parameters with the largest sensitivity.

ACPD
13, 12135–12176, 2013

1 Introduction

Radiative flux at the top of atmosphere (FNET) is important to the Earth climate system and drives surface temperature change (Forster et al., 2007). Changes of Earth system components, such as greenhouse gases, aerosols, clouds, and land surface properties, can alter the FNET (Anderson et al., 2010, 2012). These changes are normally expressed in terms of radiative forcing, an index measuring the alteration of incoming and outgoing energy in the Earth-atmosphere system due to a given factor as a potential climate change mechanism. Due to the complexity of the Earth-atmosphere system, the quantification of radiative forcing has proven difficult and is limited by uncertainties (Forster et al., 2007). For example, the fourth assessment report of the Intergovernmental Panel on Climate Change (IPCC AR4) reported a total anthropogenic radiative forcing of 1.6 $W m^{-2}$ with an uncertainty range of 0.6–2.4 $W m^{-2}$. Quantifying and reducing the uncertainties of radiative forcing in Earth system components is necessary to improve the projection of future climate change (Kiehl, 2007).

Cloud and aerosol are two of the most important and uncertain agents in the climate system influencing the Earth energy balance. Understanding the roles of clouds and aerosols in the climate system has been significantly improved, but they remain two of the dominant sources of uncertainty in climate models (Schwartz, 2004; Collins et al., 2006; Lohmann et al., 2007; Ramanathan and Carmichael, 2008; Lohmann and Ferrachat, 2010; Lee et al., 2012). Clouds affect the climate system by modifying radiation fluxes through the atmosphere (Loeb et al., 2009). Aerosols can interact with the solar radiation through absorption and scattering and to a lesser extent with the terrestrial radiation (Forster et al., 2007). Aerosol can also serve as cloud condensation nuclei (CCN) and/or ice nuclei (IN) to influence cloud albedo and lifetime (e.g., Lohmann and Feitcher, 2005). Many cloud and aerosol processes are complicated, and cloud and aerosol amounts and properties vary extremely in space and time (e.g., Zhao et al., 2013). So far, global climate models cannot fully treat details of the physical processes governing cloud and aerosol formation, lifetime, and radiative effects due to insuffi-

ACPD
13, 12135–12176, 2013

cient understanding or computational limitation. Therefore, global climate models represent these processes using simplified parameterizations with empirical parameters with large uncertainties. Moreover, the parameterizations normally vary significantly from one model to another (Boucher and Lohmann, 1995; Penner et al., 2006; Ghan and Easter, 2006; Bauer et al., 2008; Fast et al., 2011). In addition to the internal model parameters related to physical and chemical processes, aerosol radiative forcing is also sensitive to external factors such as emissions (Dentener et al., 2006; Textor et al., 2006). IPCC AR4 reported the estimated aerosol radiative forcing (including both direct and first indirect effects) with a wide uncertainty range from -1.8 to $-0.1\,\mathrm{W\,m^{-2}}$. This uncertainty is mainly due to structural (model-to-model) differences and aerosol emission uncertainties.

In the past two decades, most efforts to define model uncertainty of radiative forcing have focused on multi-model inter-comparisons (e.g., Penner et al., 2006; Textor et al., 2006; Quaas et al., 2009). Although this approach provides useful information about model diversity but limits estimating the parametric sensitivity in the individual models (Jackson et al., 2004, 2008; Haerter et al., 2009; Lohmann and Ferrachat, 2010). In this study, we focus on evaluating the parametric sensitivity in an individual model, quantifying and attributing variance in simulated FNET due to perturbation of the most uncertain parameters related to cloud microphysics and aerosol processes and emissions, in the Community Atmosphere Model version 5 (CAM5). CAM5 is a community model (http://www.cesm.ucar.edu/models/cesm1.0/cam/) and has been used to estimate radiative forcing of aerosols and their impact on the climate system (e.g, Ghan et al., 2012; Liu et al., 2012; Gettelman et al., 2012; Hurrell et al., 2013). As CAM5 is an important component of the Community Earth System Model (CESM), quantifying the sensitivity of simulated FNET to parametric and emission perturbations can improve our understanding of uncertainty in CESM.

Sensitivity analysis (SA) can quantify model parametric sensitivity and identify the processes that have the largest contribution to it. SA uses standard "one-at-a-time" (OAT) sensitivity tests that systematically investigate the model behavior departed from

ACPD
13, 12135–12176, 2013

the baseline simulation by varying one parameter at a time. However, OAT tests cannot take parameter interactions into account, and they consider only a small fraction of the total parameter uncertainty space (Saltelli and Annonia, 2010). A more comprehensive approach is to populate the statistical distribution of model outputs by sampling hundreds or thousands of possible parameter values. The SA, such as analysis of variance and variance decomposition, then uses output distributions to understand contribution of each parameter to the overall variance.

To date, there is no such comprehensive SA study on CAM5 parameters related to cloud microphysics and aerosol to our knowledge. From the limited number of studies performed to date, it also is not clear which parameters associated with cloud microphysics and aerosol parameterizations or with aerosol and precursor emissions are most responsible for the uncertainty in the CAM5-simulated climate variables. In this study, we adopted an SA framework that integrates an exploratory sampling approach (quasi-Monte Carlo), and a generalized linear model analysis, for SA of CAM5 simulated-variance of the present-day FNET, with the focus on evaluating the sensitivities associated with the cloud microphysics and aerosol parameters. This paper is organized as follows. Section 2 and 3 detail the CAM5 model and the SA methodology used in this study. The SA of the CAM5-simulated variance of FNET associated with cloud microphysics and aerosol parameters is presented in Sect. 4. The findings are summarized and discussed in Sect. 5.

2 Methodology

2.1 Model description

The model used in this study is CAM5. The treatment of aerosols in this model is described in Liu et al. (2012). The three-mode version of the modal aerosol scheme (MAM3) in CAM5 is used in this study and features Aitken, accumulation, and coarse modes. Aerosol components are internally mixed in each mode. The mass and num-

ACPD
13, 12135–12176, 2013

ber concentrations in each mode are updated during the simulation. The size distribution of each mode is assumed to be log-normal and the σ of log-normal distribution is prescribed. Fifteen aerosol species are transported. The model includes important processes that influence the aerosol life cycle such as emission, dry and wet deposition, gas- and aqueous-phase chemistry, nucleation, coagulation, and condensational growth.

The CAM5 model treat physical processes in stratiform and cumulus clouds in separate parameterizations. Mass and number concentrations of cloud droplets and ice crystals and of rain and snow are predicted and diagnosed, respectively, in the stratiform cloud microphysics parameterization (Morrison and Gettelman, 2008; Gettelman et al., 2008, 2010). Stratiform cloud macrophysics is described by Gettelman et al. (2010). Aerosol influence on stratiform cloud microphysics is based on Abdul-Razzak and Ghan (2000) for the droplet activation and on Liu et al. (2007) for ice nucleation. The shallow cumulus clouds are treated as Park and Bretherton (2009). The deep convective clouds are parameterized following Zhang and McFarlane (1995) but has been modified by Neale et al. (2008). Aerosol cannot directly affect cumulus cloud microphysics but can be scavenged by convective clouds in current version of CAM5.

The Rapid Radiative Transfer Model for GCMs (RRTMG) is used for longwave and shortwave radiative transfer (Mlawer et al., 1997; Iacono et al., 2000). Aerosol optical properties are calculated following Ghan and Zaveri (2007). The Optical Properties of Aerosols and Clouds (OPAC) dataset (Hess et al., 1998) is used for refractive indices for most aerosol components, but the value $(1.95 + 0.79i)$ from Bond and Bergstrom (2006) is used for black carbon (BC). The liquid and ice cloud optical properties are calculated following Morrison and Gettelman (2008) and Mitchell (2000 and 2006), respectively. More details on CAM5 are available at http://www.cesm.ucar.edu/models/cesm1.0/cam/.

ACPD
13, 12135–12176, 2013

2.2 Experiment design

In this study, we use 1.9° latitude × 2.5° longitude resolution with 30 vertical layers. Each simulation is performed with the Atmosphere Model Intercomparison Program (AMIP) configuration that uses prescribed greenhouse gas concentrations and sea surface temperature for the years from 2000 to 2004. Emissions are from the IPCC AR5 estimates (Lamarque et al., 2010). Simulations are run for 2000–2004 with only the final four years (2001–2004) analyzed. The performance of MAM3 aerosol module in year 2000 simulations of CAM5 has been evaluated by Liu et al. (2012).

2.3 SA framework

2.3.1 Parameterization

While many parameters likely contribute to uncertainties in CAM5, this study focuses on 16 parameters related to cloud microphysical processes and aerosol physics and chemistry processes that include cloud ice microphysics, cloud droplet activation, aerosol wet scavenging, solar radiation absorption by dust, and emission fluxes and size distributions (see the descriptions shown in Table 1). These uncertain parameters are chosen by model developers of CAM5 and also agree with previous studies. For example, the ice falling speed (ai) has been identified as the second most influential parameter to the climate sensitivity (Sanderson et al., 2008) and has a significant effect on cloud radiative forcing (Mitchell et al., 2008). The parameter for auto-conversion of cloud ice to snow (dcs) is one of the most effective tuning parameters in CAM5 for the radiative budgets. Both subgrid in-cloud vertical velocity (wsubmin) (Golaz et al., 2011) and cloud droplet number lower limiter (cdnl) (Hoose et al., 2009) both play crucial roles on cloud droplet number concentration and aerosol indirect effect. Tuning parameters that control wet removal of aerosols (sol_facti and sol_factic) remains a key source of uncertainty in global aerosol models, which strongly affects the vertical distribution and long-range transport of submicron aerosols (Vignati et al., 2010; Wang et al., 2013).

ACPD
13, 12135–12176, 2013

Dust absorption property (refindex_dust_sw) is a key quantity with large uncertainty for aerosol optical properties (Zhao et al., 2011). There are large uncertainties in the emissions of sea salt and mineral dust (emis_SEAS and emis_DUST) (Textor et al., 2006), as well as secondary organic aerosol (SOA) formation (emis_SOAg) (e.g., Spracklen et al., 2011) in global aerosol models. In addition, we perturb the emission rate of anthropogenic SO_2 (emis_SO2) and the molar fraction of it directly emitted as sulfate (emis_SO4f), as well as the emission rate of anthropogenic carbonaceous aerosols (emis_POM and emis_EC) and the emission size of aerosols in accumulation mode controlled by the number concentration (emis_num_a1_surf).

These 16 parameters can show perturbations in simulated variance of FNET stemming from perturbations in internal parametric variability (first 8 parameters in Table 1) and emission scenarios and uncertainties (the last 8 parameters in Table 1). The perturbation ranges (from minimum to maximum) of these 16 parameters are chosen by CAM5 model developers (shown in Table 1). These ranges reflect our best knowledge of parameter uncertainties in aerosol (R. C. Easter and S. J. Ghan, personal communication, 2012) and cloud microphysics parameterizations (H. Morrison, personal communication, 2012) in CAM5.

2.3.2 Quasi Monte Carlo sampling

In this study, the probability distribution of each model parameter is assumed to be uniform within its uncertainty range (from minimum to maximum). Due to the high dimensionality of the parameter space and computational demand, efficient and reliable SAs must be used to explore the parameter space. Systematic sampling techniques, such as Simpson's rule, are insufficient (Tarantola, 2005). Traditional Monte Carlo (MC) sampling is also insufficient with many gaps and clumps, which may result in missing and/or duplicated numerical simulations. A quasi-Monte Carlo (QMC) sampling approach guarantees good dispersion between samples (Caflisch, 1998) and therefore is adopted in this study. QMC sampling can achieve good uniformity even in higher-dimensional projections by filling gaps and avoiding clumps in the sampling points,

ACPD
13, 12135–12176, 2013

achieving better performance than MC and Latin hypercube sampling (LHS) in general (Wang and Sloan, 2008; Hou et al., 2012). QMC sampling produces a series of samples with controlled deterministic inputs instead of random ones.

The number of QMC samples normally is a power of 2 and usually is chosen as a trade-off between computational time and numerical error. It is important to make sure there is no significant under-sampling issue that may affect the reliability of the developed relationships between the output responses (e.g., FNET) and the independent variables (see Table 1). Therefore, tests were performed to determine the number of QMC samples (up to 256 samples) needed for reliable outputs. Based on the tests, we have confirmed that output statistics and sensitivity based on 128 samples are comparable to those based on 256 samples (not shown). In this study, the analysis results from 256 samples are used.

2.3.3 Statistical analysis

After CAM5 simulations are completed for each combined parameter set, we perform statistical analyses of the output responses (e.g., variance of FNET) to these internal and external parameters, including their linear/nonlinear and interaction effects, via generalized linear model (GLM) analysis. The GLM performs statistical tests of the significances of the input parameters. These statistical significance values are used to rank the contributions of inputs to the overall variability of each output response through a full, variance-based SA. The SA quantifies the simulated variance of FNET that results from the perturbations of selected model parameters and identifies the significant parameters for FNET variance in global or specific regions. A GLM is fitted with the following starting model:

$$Y^i = \beta_0 + \sum_{j=1}^{n} \beta_j \cdot p_j^i + \sum_{j=1}^{n} \sum_{k=1}^{n} \beta_{j,k} \cdot p_j^i \cdot p_k^i + \varepsilon_i, \quad \varepsilon_i \sim^{iid} N(0, \sigma^2)$$

ACPD
13, 12135–12176, 2013

where p_j^i represents the ith realization of the jth parameter; Y_i represents the ith response variable (e.g., FNET); β_j and $\beta_{j,k}$ represent the coefficients of linear and two-way interaction terms, respectively; and ε_i denotes the residual for the ith realization. This model assumes the response variable (e.g., FNET) is a combination of these aforementioned parameters, and the model-fitting residuals ε_i follow independent normal distributions with zero mean and unit variance.

The GLM evaluates the statistical significance of the input parameters through null hypothesis tests, which proposes that no statistical significance exists in a set of given observations. The t statistic value for testing the null hypothesis that the regression coefficients $\widehat{\beta}_i$ is zero (such that the corresponding parameter is likely insignificant) is given by $t = \widehat{\beta}_i / \mathrm{SE}(\widehat{\beta}_i)$. The P value for the test and interpreted variance (fitted sum squares) by each term also are computed. The coefficient of determination (R^2) of model fitness also is computed as the fitted variance relative to the overall variance of each output response. A parameter is considered to be significant if the corresponding P value is larger than a chosen significance level of the test (e.g., 0.05 or 0.1) (McCullagh and Nelder, 1989; Venables and Ripley, 2002). The interpreted variances are used to study and rank the relative contributions of each input parameter.

To evaluate the overall magnitude and global/localized variability due to the perturbations/uncertainties in the input parameters, ensemble output responses (e.g., FNET) are summarized. To demonstrate not only the global mean sensitivity but also sensitivity patterns at different locations, we consider both the global averaged and localized (e.g., at each grid point) output (e.g., FNET) as response variables in this study.

3 Results

3.1 Global Mean FNET Sensitivity

Figure 1 shows the annual-mean anomalies of global mean FNET variance in response to the perturbations of 16 parameters from the 256 CAM5 simulations as described

ACPD
13, 12135–12176, 2013

above. These 256 simulations are equally grouped into 8 sub-ranges for each input parameter (i.e., 32 values are averaged in each sub-range) to rule out effects from the perturbation of other parameters. The minimum and maximum global mean FNET within each sub-range are shown as vertical bars. The anomalies are calculated by subtracting the 256-simulation mean from each individual simulation. The range of FNET in each sub-range of an individual input parameter results from perturbations of other parameters because the parameters are perturbed simultaneously during the sampling. The figure clearly shows how input perturbations propagate through CAM5 to output variance. It also shows how the FNET response behaves when parameters fall in different sub-ranges.

Among the 256 simulations, FNET ranges from $-9.8\,\mathrm{W\,m^{-2}}$ to $3.5\,\mathrm{W\,m^{-2}}$ in response to the perturbations of the input parameters, compared to the default CAM5-simulated FNET of $1.9\,\mathrm{W\,m^{-2}}$. To better understand FNET responses to the perturbations of input parameters, two components of FNET, direct change of radiation fluxes in clear sky (FNETC) and indirect cloud-induced change of radiation fluxes (net shortwave and longwave CF) (FNET = FNETC + CF), are also shown in Fig. 1. FNETC ranges from $27.1\,\mathrm{W\,m^{-2}}$ to $32.2\,\mathrm{W\,m^{-2}}$and CF ranges from $-39.0\,\mathrm{W\,m^{-2}}$ to $-26.8\,\mathrm{W\,m^{-2}}$ in the 256 simulations in response to the perturbations of input parameters, corresponding to the default CAM5 simulated FNETC of $30.3\,\mathrm{W\,m^{-2}}$ and CF of $-28.4\,\mathrm{W\,m^{-2}}$. The CF variance is much larger than that of FNETC and dominates that of FNET.

To quantify the relative contribution of each parameter perturbation to the overall variance of FNET, FNETC, and CF, the GLM is applied. The *P* value is obtained from the GLM analysis as explained above (Sect. 2.3.3). When a *P* value is larger than a significance level of 95 %, i.e., 0.05, the corresponding variable (input parameter) change is relatively insignificant with its assigned perturbation. Using this methodology, we have identified the significant parameters for the variance of FNET, FNETC, and CF. Figure 2 shows the correspondence of global mean FNET, FNETC, and CF between the 256 CAM5 simulations and the 256 GLM predictions based on input parameters. The GLM model shown here includes both individual parameter effect and

ACPD
13, 12135–12176, 2013

their interaction. The GLM well predicts the CAM5-simulated FNET, FNETC, and CF with the coefficients of determination (R^2) of 0.98–0.99, which indicates 98–99 % of variance of CAM5 simulated FNET, FNETC, and CF is explained by the GLM.

With the GLM, the relative contribution (in percentage) of each input parameter perturbation to the overall variance of FNET, FNETC, and CF can be quantified, as shown by the numbers in Fig. 1. The relative contributions indicate that the perturbation of dcs is the largest contributor (30.4 %) to the total variance of FNET, followed by that of wsubmin (26.8 %), emis_SEAS (12.6 %), sol_factic (11.1 %), cdnl (5.7 %), and other parameters with contributions less than 5 %. In addition, the parameters with contributions that are 95 % statistically significant are highlighted in red (shown in Fig. 1). Perturbations of most internal parameters (i.e., model parameters), except refindex_dust_sw are 95 % statistically significant to the variance of FNET. For external parameters (i.e., emission parameters), perturbations of sea-salt, SOA precursors, SO_2, and POM emissions and the size distribution of emitted fossil fuel carbonaceous aerosols (POM and BC) are 95 % statistically significant, but not the emissions of dust and BC and the fraction of sulfate aerosol in total sulfur emission.

In general, FNET increases with dcs and sol_factic, but decreases with ai, cdnl, wsubmin, emis_SEAS, emis_SO2, emis_POM, and emis_num_a1_surf. As the largest contributor to the FNET variance, dcs affects radiative fluxes at the TOA under both clear-sky and cloudy-sky conditions (i.e., FNETC and CF). The perturbation of dcs not only significantly contributes to CF variance by 55.5 %, but also substantially contributes to FNETC variance by 25.1 %. In general, FNETC can be changed through direct scattering of incoming SW or indirect trapping of outgoing LW from surface temperature feedback. The CF change can be decomposed into SWCF and LWCF changes. Figure 3 shows the anomalies of global mean variance of LW and SW potion of FNETC and CF and Fig. 4 shows the anomalies of global mean variance of liquid water path (LWP), ice water path (IWP), water vapor path (WVP), and surface temperature (TSK), respectively, in response to the perturbations of the 16 input parameters from the 256 CAM5 simulations. The CF increases with dcs (i.e., increasing dcs leads

ACPD
13, 12135–12176, 2013

to warming), mainly through LWCF (51.4 %, increase with dcs) with a relatively small portion (2.5 %) from SWCF. Increasing dcs reduces the rate of auto-conversion of cloud ice to snow, and thus increases the cloud ice water path (IWP) with a dominant contribution (99.1 %) to the IWP variance. The increasing IWP traps more outgoing LW and hence increases LWCF (Fig. 3) and TSK (Fig. 4). The overall variance of TSK is 0.5 K with 52.7 % contribution from the perturbation of dcs. The increase of dcs has negligible impact on LWP. The perturbation of dcs significantly affects LWFNETC variance with contribution of 86 % and has negligible impact on SWFNETC. The increase of dcs reduces LWFNETC (more negative) through increasing outgoing LW radiation under clear-sky via surface temperature feedbacks (Fig. 4). The increase of TSK also leads to the increase of atmospheric water vapor content. This study confirms why dcs has been used as one of the most effective tuning parameters for the TOA radiative forcing in the CAM5 development (Gettelman et al., 2010).

The effect of wsubmin, the second largest contributor, is different from that of dcs. The relative contribution of perturbation of wsubmin to FNETC variance is negligible (close to 0 %) compared with that of 25.9 % to CF variance, indicating that wsubmin reduces FNET primarily by reducing CF. CF significantly decreases with wsubmin primarily due to reduction of SWCF (more negative). The increase of wsubmin enhances the activation fraction of aerosols to cloud droplets, and thus increases the albedo through increasing the cloud droplet number concentration (i.e., aerosol first indirect effect) and lifetime of liquid clouds (i.e., aerosol second indirect effect). While the perturbation of wsubmin significantly contributes to the LWP variance (33.9 %) via the aerosol second indirect effect, it has negligible impact on IWP variance. The perturbation of wsubmin also changes the surface temperature through modifying clouds. However, it mainly affects liquid clouds and has a relatively smaller impact on surface temperature than dcs. Therefore, wsubmin has a much smaller impact on LWFNETC and hence on FNETC compared to dcs. Generally, wsubmin mainly affects liquid cloud that has larger impact on incoming SW, while dcs primarily affects ice clouds that have a larger impact on outgoing LW. Although both parameters affect clouds and significantly impact the CF,

ACPD
13, 12135–12176, 2013

their feedbacks are different since the effect of clouds on TOA radiation depends on their heights and thicknesses (i.e., low clouds lead to cooling and high clouds lead to warming).

Compared to the perturbation of dcs, the perturbations of the other three cloud microphysics related parameters, ai, as, and cdnl, contribute merely 2.8 %, 1.5 %, and 5.7 %, respectively, to the FNET variance. The perturbations of ai and as contribute to 26.7 % and 15.1 %, respectively, of LWCF variance, and to 11.2 % and 21.5 %, respectively, of SWCF variance. Increasing ai and as reduces the IWP (through ice and snow sedimentation) and LWP (through mixed-phase microphysical processes), weakens the LWCF and SWCF at a similar magnitude, and thus results in a relatively small impact on CF and FNET. Increasing both ai and as reduces TSK, but has relatively small impact on LWFNETC and SWFNETC. Varying cdnl has a much larger impact on SWCF (17.1 %) than on LWCF (2.9 %) and a negligible impact on FNETC. Increasing cdnl significantly increases the LWP and hence CF by increasing the cloud droplet number concentration to the lower limiter at remote regions where cloud droplet number is limited by the availability of CCN. Increasing the solubility factor of interstitial aerosols (with respect to convective cloud-borne aerosol) (sol_factic) increases the efficiency of wet removal of aerosols by convective rain, and thus reduces overall aerosol concentrations, as well as cloud albedo and the LWP (e.g., Wang et al., 2013). Therefore, the increase of sol_factic enhances SWFNETC with a contribution of 16.6 % to the SWFNETC variance. The CF (mainly from SWCF) also increases with sol_factic. However, the solubility factor of stratiform cloud-borne aerosols (sol_facti) has a negligible impact on both FNETC and CF likely because cloud-borne aerosols in stratiform clouds already experience too fast wet scavenging in CAM5 (Liu et al., 2011). The increase of refindex_dust_sw (visible imaginary refractive index of dust) augments global mean SWFNETC due to the enhancement of dust SW absorption, but this has a statistically insignificant impact on global mean FNET with its perturbed range (0.001–0.01).

Among the external parameters (i.e., emission parameters), increasing the mass emissions of sea salt, dust, anthropogenic SO_2, and POM as well as increasing the

ACPD
13, 12135–12176, 2013

number emission of aerosol in accumulation mode (by reducing the emission size) increases the aerosol optical depth and CCN number concentrations. The perturbation of emis_SEAS (i.e., sea salt emission) contributes most significantly (12.6 %) to the global mean FNET variance, mostly through its contribution (45.2 %) to the FNETC variance. The increase of sea salt emission reduces FNETC via its impact on SWFNETC by scattering more solar radiation. Other emission parameters including dust and anthropogenic emissions have much smaller impact on FNET variance than sea-salt emission, likely due to their emissions primarily over the continents where aerosol concentrations are relatively more abundant. Contributions of emissions perturbations (except emis_SO4f) are also normalized by their perturbing scale (i.e., perturbation range of each emission parameter). The results are summarized in Table 2. It shows that the dominant contribution of the emis_SEAS perturbation among emission parameters to global mean FNET variance stems from its contribution to the global mean FNETC. In terms of CF, perturbation of each emission has a comparable contribution.

By using the SA approach in this study, we are able to quantify the interactions among the 16 input parameters. When a perturbation of one parameter enhances or weakens the sensitivity of another parameter, interactions occur. Figure 5 shows the relative contributions of perturbations of each parameter and their interaction effect to the FNET, FNETC, and CF variance. The main effect (i.e., without interaction effect) of perturbations of individual parameters contributes to > 95 % of the FNET, FNETC, and CF variance, while the interaction effect contributes only ~ 3 % of their variance. In terms of the variance of global mean FNET, FNETC, and CF, the interaction effect among the selected 16 input parameters is inconsequential in CAM5.

3.2 Spatial distribution of FNET and its uncertainty

Both the global mean change of FNET and changes in its spatial distribution are important for driving climate change, particularly at the regional scale. Figure 6 shows the spatial distribution of variance of FNET, FNETC, and CF in response to the perturbations of 16 input parameters from 256 CAM5 simulations. The FNET variance shows

ACPD
13, 12135–12176, 2013

a large spatial variability. Relatively large FNET variance occurs over the southern oceans (south of 60° S), northern Pacific, northern Atlantic, East Asia, Tibetan Plateau, South and North Africa, and South America. The FNET variance over the polar-regions is relatively small, particularly over the Antarctic. The CF variance dominates the FNET variance over most regions, which is consistent with the analysis of global mean FNET. The relatively large FNET variance over the oceans, South Africa, and South America is mainly due to the large variance of CF over these regions. Relatively large FNETC variance occurs over North Africa, East Asia, and the Tibetan Plateau. It is interesting to note that FNETC also has relatively large variance over the Arctic, where the variance of CF and FNETC offsets each other so that the FNET variance is small. These features of spatial variability will be discussed in the analysis of the contribution of each parameter perturbation in following.

To quantify the variance contributions from the 16 input parameters, the GLM analysis is conducted for the FNET of each grid as it is applied for the global mean FNET in Sect. 3.1. Figure 7 shows the spatial distributions of R square of the GLM models for FNET, FNETC, and CF. In general, GLM models can well predict FNET, FNETC, and CF variance over most regions at latitudes lower than 70° with high R square values of > 0.9. The regions with relatively lower R square values ($0.5 \sim 0.8$), e.g., higher latitudes and Australia, generally also have smaller variance of FNET, FNETC, and CF (Fig. 6). Therefore, they have less interest in terms of investigating variance sources. Figure 8 shows the global spatial distribution of absolute contributions of the 16 input parameters to the FNET variance from the 256 CAM5 simulations estimated by the GLM. Note that the FNET variance in any given grid box can be affected not only by the localized processes but also by the processes occuring at other grid boxes. For example, the aerosol at any location has contributions from both long-range transport and physical and chemical transformations, so the impact of an aerosol related parameter in a given grid box depends on the integrated effect of that parameter. The global spatial distributions of absolute contributions of the perturbations of 16 input parameters to

ACPD
13, 12135–12176, 2013

the FNETC and CF variance, respectively, from the 256 CAM5 simulations estimated by the GLM are shown in Figs. 9 and 10.

Among all parameters, the perturbation of dcs is the largest contributor to the FNET variance over many regions of the globe, such as the North Pacific and the southern oceans (50° S–70° S), with relative contributions of > 50 % (refer to Fig. S1 in the Supplement). dcs also makes significant contributions to the FNET variance over the Tropical Pacific, North Atlantic, and North and South America. The contribution of dcs perturbation to the FNET variance primarily is from its impact on CF over most regions, which is consistent with the impact of dcs on global mean FNET variance. The primary impact of dcs stems from its effect on IWP over regions where there is a large amount of ice clouds (see Fig. S2 in the Supplement). The effect is different over the Arctic. The dcs affects the FNET variance mainly through its impact on TSK and hence FNETC over the Arctic (Fig. S3 in the Supplement). The relative contribution of perturbations of as and ai to the FNET variance is much less than that of dcs over most regions and is mainly due to their impact on CF. The perturbation of cdnl contributes < 10 % to the FNET variance over most regions of the globe and occurs mainly due to its impact on CF. The four cloud microphysics parameters are the main contributors to the FNET variance over polar regions because of their impact on liquid (from cdnl) and ice (from dcs, ai, and as) clouds (refer to Supplement).

The perturbation of wsubmin significantly contributes to the FNET variance over East Asia, the Tropical Pacific, and the outflow regions of East Asia over the Pacific and North America over the Atlantic. The wsubmin impact is mainly through its impact on LWP and thus CF due to the increase in cloud droplet number concentrations and thus aerosol indirect effect over regions where there are frequent occurrences of liquid-containing clouds (e.g., along the North Pacific and Atlantic storm tracks) and sufficient amount of CCN (see Fig. S4 in the Supplement). The significant contribution of sol_factic perturbation to the FNET variance stems chiefly from its impact on CF at mid- and lower latitudes, where the convections are more likely to occur and more aerosols are subject to wet removal. It has the largest contribution over the Pacific Ocean near

ACPD
13, 12135–12176, 2013

the Amazon Basin of South America. The absolute contribution of sol_facti perturbation to the FNET variance is small (1–5 %) throughout the globe. The perturbation of refindex_dust_sw is the largest contributor (> 50 %) to the FNET variance over the Saharan desert and Asian deserts. Its impact is mostly confined near the desert regions. It affects the FNET variance principally through its impact on FNETC through the direct effect of dust but also partly due to its impact on CF via the semi-direct effect of dust.

The perturbation of dust emission (emis_DUST) contributes 10–30 % to the FNET variance over the Saharan and Asian deserts mainly through its impact on FNETC. The contribution is mostly confined to the desert regions, but the FNET variance over the North Atlantic is also affected due to the Sahara Air Layer (SAL) (e.g., Dunion and Velden, 2004). The perturbation of sea-salt emission (emis_SEAS) dominates the FNET variance over the oceanic regions at middle and lower latitudes with strong sea-salt emissions. Its contribution is primarily stems from its impact on the FNETC variance, except over the Southern Ocean at ∼ 60° S, where its contribution to the CF variance by acting as CCN is larger.

The contributions of perturbations of anthropogenic emissions are larger over continents than over oceans. The perturbation of anthropogenic SO_2 emission (emis_SO2) has significant impact on the FNET variance over the Northern Hemisphere (NH), in particular over the North Pacific and Atlantic where its contribution reaches 40 % of the FNET variance (see Fig. S1 in the Supplement). The significant impact of emis_SO2 (anthropogenic SO_2 emission) occurs over both the source (continent) and remote (oceanic) regions. Over the continent, emis_SO2 perturbation contributes to the FNET variance principally through FNETC (direct effect) while over the ocean it is mainly through CF (indirect effect). Among all the anthropogenic emissions, the perturbation of BC emission is the largest contributor (> 30 %) to the FNET variance over East China and North India. The emis_BC also affects CF through semi-direct effect of BC. The perturbations of emis_POM and emis_num_a1_surf lead to significant FNET variance through CF over the biomass burning regions and NH continental outflows. The perturbation of emis_SOAg leads to relatively small FNET variance through FNETC with

ACPD
13, 12135–12176, 2013

relative contributions of ∼10 %. The contribution of emis_SO4f perturbation is negligible throughout the globe. The impact of these emission parameters on the FNETC variance is larger over aerosol source regions (i.e., continent), while their impact on the CF variance is larger over the continental outflow regions over ocean, indicating the higher susceptibility of marine clouds to aerosol perturbations. Note that the relative contributions of emission perturbations to the FNET variance are dependent on the prescribed perturbation range of emissions. In one SA, the contributions of emission perturbations are normalized by the standard deviations of emission parameters. In this case, the contribution is much less dependent on the perturbation ranges. We found that the spatial distributions of normalized contributions (Fig. S5 in the Supplement) are not significantly different from the ones shown in Fig. S1 for relative contributions of FNET variance from the 16 selected input parameters. Notably, it is difficult to normalized contributions from all parameters because cloud microphysics parameters have different physics meanings and units from those used for emissions.

Similar to the analysis of interaction effects for global mean FNET (Fig. 5), the individual and interaction effects analyzed using the GLM are shown in Fig. 11. The analysis is conducted for each grid globally. The GLM predicted total variance of FNET is similar to the CAM5 simulated variance (Fig. 6) and consistent with the high R square values (Fig. 7). In general, individual effect dominates the total effect. The interaction effect is relatively small over most regions of the globe, except the polar regions and Australia, where the interaction contribution can reach more than 50 %. The reason for the large impact of interaction effects in these regions is unknown. However, the FNET variance is relatively small over these regions. The parameter interaction contributes to < 15 % of the FNET variance over most regions of the globe. The spatial distribution of the interaction effect on FNETC and CF are consistent with that of FNET.

ACPD
13, 12135–12176, 2013

4 Conclusions and discussion

In this study, we developed and applied an SA framework to analyze the variance of simulated radiative flux at the top of atmosphere (FNET) in the present-day climate due to perturbations of model internal parameters related to cloud microphysics and aerosol processes and external parameters related to aerosol and its precursor gas emissions in the state-of-the-art global climate model CAM5. The analysis demonstrates the high sensitivity of FNET to 16 input parameters within the perturbed ranges. FNET varies from $-9.8\,\mathrm{W\,m^{-2}}$ to $3.5\,\mathrm{W\,m^{-2}}$ in the 256 simulations in response to the perturbations of input parameters, compared to the CAM5-simulated FNET of $1.9\,\mathrm{W\,m^{-2}}$ with default parameter values. The analysis indicates a change in FNET of -11.7–$1.6\,\mathrm{W\,m^{-2}}$ (compared to the FNET from standard CAM5 simulation) that is much larger than the range of -1.8–$-0.1\,\mathrm{W\,m^{-2}}$ from IPCC AR4 report for the aerosol radiative forcing. This FNET change is dominated by the change of CF, indicating the importance of improving cloud parameterizations in CAM5. We certainly realize here that this large FNET change is dependent on the perturbation range assigned by the model developers.

Our variance-based analysis shows that the GLM reproduces global mean and spatial patterns of CAM5-simulated variance of FNET and its components, CF and FNETC. The results show that the global mean FNET variance is dominated by the CF variance with the assigned parameter ranges. Most selected cloud microphysics and emission related parameters are found to have statistically significant impact on the global mean FNET. The results confirm dcs (i.e., auto-conversion size threshold for ice to snow) as one of the most effective tuning parameters for the TOA radiative forcing in CAM5. Compared to dcs, the other three cloud microphysics parameters associated with the falling speed of cloud ice and snow and the limiter of cloud droplet number have a smaller impact on the global mean FNET. The increase of wsubmin (i.e., minimum limit of subgrid in-cloud vertical velocity) increases the albedo through increasing the cloud droplet number concentration (i.e., aerosol first indirect effect) and lifetime of liquid clouds (i.e., aerosol second indirect effect). The emission parameters are found

ACPD
13, 12135–12176, 2013

to have relatively small impact on the global mean FNET except the one related with sea salt emission because their impact is mostly confined over the source region. This SA framework is also able to quantify the interactions among the input parameters. However, the SA indicates much smaller interaction effect among the selected 16 parameters compared to their individual effect on the global mean FNET.

In terms of spatial distribution, the FNET variance due to the parametric perturbation has strong heterogeneous geographic distribution. The spatial distribution of the FNET variance contribution of some input parameters has a clear localized effect that primarily impacts over the area where that parameter is in effect. For example, the FNET variance contribution from dcs perturbation mainly is over the ice-cloud regions. The contribution from perturbation of sea salt and dust emissions shows up primarily in windy marine and desert regions, respectively. However, the perturbation in some parameters has a non-local impact on FNET variance. For example, aerosol wet scavenging can affect the FNET variance in regions without clouds, and the anthropogenic emission of SO_2 influences FNET over the remote oceanic regions. The parameter interaction is a relatively small contributor to the FNET variance over most regions of globe.

Some clarification of the results in this study should be made. First, the uncertain range of anthropogenic aerosol and precursors emissions may be different from the perturbation range we prescribed here. The investigated ranges of emissions are selected for SA rather than uncertainty quantification. Second, the impact of parametric perturbation on the FNET variance does not include the sea surface temperature (SST) feedbacks due to the prescribed SST used in this study, although it is a standard method to calculate the radiative flux perturbation with prescribed SST. Third, in this study we examine the uncertain parameters related to cloud microphysics and aerosol processes as the first step. We note that there still are other uncertainty parameters in CAM5 that can affect the modeled FNET. However, the approach in this study is ready to be extended to a larger set of parameters for other parameterizations and eventually also other models, providing a framework for the quantifiable analysis of model sen-

ACPD
13, 12135–12176, 2013

sitivity. Finally, the conclusions in this study are limited to the CAM5 model, but such systematic studies may be useful for other GCMs as well. In fact, some previous studies also investigated the impact of uncertainty parameters in individual climate models (e.g., Lohmann and Ferrachat, 2010; Lee et al., 2012). Lohmann and Ferrachat (2010) used the OTA SA method to investigate the impact of important tunable parameters associated with the ice cloud optical properties and the convective and stratiform clouds on the present-day climate in a global climate model, and concluded that tuning of these parameters has a negligible influence on the anthropogenic aerosol effect. Lee et al. (2012) applied a statistical emulation technique in a global chemical transport model to quantify uncertainty in simulating CCN concentrations, and concluded that the modeling uncertainty of CCN is only sensitive to emission parameters in polluted regions but mainly results from the uncertainties of parameters associated with model processes in all other regions. These findings have benefited the climate modeling community.

This study highlights that the next step of reducing modeling uncertainty through calibration needs a complete understanding of the model behavior within the parameter uncertainties (e.g., identifying a set of model parameters that best matches observations within defined criteria) (Yang et al., 2012, 2013). Although anthropogenic and natural emissions are uncertain and important to accurately simulate FNET change, particularly at the regional scale, within the ranges (see Table 1) investigated in this study, the impact of the model internal parametric uncertainties can be higher in terms of simulating global mean CF and FNET. More studies are needed to improve the cloud microphysics and sub-grid cloud variability in GCMs. Analysis of spatial distribution of FNET variance can provide useful guidance for planning measurement campaigns to efficiently reduce modeling uncertainty of the FNET change. In addition, this study indicates the high sensitivity of FNET to model internal parameters. Although the future climate change is commonly projected by a climate model with its "standard" set of internal parameters that can be used to reproduce historical climate, there may be

ACPD
13, 12135–12176, 2013

another set of internal parameters existing to reproduce similar historical climate but significantly different future climate.

Supplementary material related to this article is available online at: http://www.atmos-chem-phys-discuss.net/13/12135/2013/acpd-13-12135-2013-supplement.pdf.

Acknowledgements. This research was supported by the Office of Science of the US Department of Energy (DOE) as part of the Earth System Modeling Program and the Regional & Global Climate Modeling (RGCM) program. This research used computing resources from the National Energy Research Scientific Computing Center, which is supported by the DOE Office of Science under Contract No. DE-AC02-05CH11231. Pacific Northwest National Laboratory is operated by Battelle Memorial Institute for the DOE under contract DE-AC05-76RL01830.

References

Abdul-Razzak, H. and Ghan, S. J.: A parameterization of aerosol activation: 2. Multiple aerosol types, J. Geophys. Res., 105, 6837–6844, 2000.

Anderson, B., Knight, J. F., Ringer, M. A., Desser, C., Phillips, A., Yoon, J.-H., and Cherchi, A.: Climate forcings and climate sensitivities diagnosed from Atmospheric Global Circulation Models, Clim. Dynam., 35, 1461–1475. doi:10.1007/s00382-010-0798-y, 2010.

Anderson, B. T., Knight, J. R., Ringer, M. A., Yoon, J.-H., and Cherchi, A.: Testing for the possible influence of unknown climate forcings upon global temperature increases from 1950–2000, J. Clim., 25, 7163–7172. doi:10.1175/JCLI-D-11-00645.1, 2012.

Bauer, S. E., Wright, D. L., Koch, D., Lewis, E. R., McGraw, R., Chang, L., Schwartz, S. E., and Ruedy, R.: MATRIX (Multiconfiguration Aerosol Tracker of mIXing state): an aerosol microphysical module for global atmospheric models, Atmos. Chem. Phys., 8, 6003–6035, doi:10.5194/acp-8-6003-2008, 2008.

Bond, T. C. and Bergstrom, R. W.: Light absorption by carbonaceous particles: an investigative review, Aerosol Sci. Tech., 40, 27–67, 2006.

ACPD
13, 12135–12176, 2013

Boucher, O. and Lohmann, U.: The sulfate-CCN-cloud albedo effect: a sensitivity study with two general circulation models, Tellus B, 47, 281–300, 1995.
Caflisch, R. E.: Monte Carlo and quasi-Monte Carlo methods, Acta Numerica, 7, 1–49, 1998.
Collins, W. D., Rasch, P. J., Boville, B. A., Hack, J. J., Mccaa, J. R., Williamson, D. L., and Briegleb, B. P.: The formulation and atmospheric simulation of the Community Atmosphere Model version 3 (CAM3), J. Clim., 19, 2144–2161, 2006.
Dentener, F., Kinne, S., Bond, T., Boucher, O., Cofala, J., Generoso, S., Ginoux, P., Gong, S., Hoelzemann, J., Ito, A., Marelli, L., Penner, J., Putaud, J., Textor, C., Schulz, M., van der Werf, G., and Wilson, J.: Emissions of primary aerosol and precursor gases in the years 2000 and 1750 prescribed data-sets for AeroCom, Atmos. Chem. Phys., 6, 4321–4344, doi:10.5194/acp-6-4321-2006, 2006.
Dunion, J. P. and Velden, C. S.: The impact of the Saharan air layer on Atlantic tropical cyclone activity, B. Am. Meteorol. Soc., 85, 353–365, doi:10.1175/BAMS-85-3-353, 2004.
Fast, J. D., Gustafson, Jr., W. I., Chapman, E. G., Easter, Jr., R. C., Rishel, J. P., Zaveri, R. A., Grell, G., and Barth, M.: The Aerosol Modeling Testbed: A community tool to objectively evaluate aerosol process modules, B. Am. Meteorol. Soc., 92, 343–360, doi:10.1175/2010BAMS2868.1, 2011.
Forster, P., Ramaswamy, V., Artaxo, P., Berntsen, T., Betts, R., et al.: Changes in atmospheric constituents and in radiative forcing: Climate change 2007: The physical science basis, contribution of working group I to the Fourth Assessment Report of the Intergovernmental Panel on Climate Change Cambridge University Press, edited by: Solomon, S., Qin, D., Manning, M., Chen, Z., Marquis, M., et al., UK and New York, NY, USA, 2007.
Gettelman, A., Morrison, H., and Ghan, S. J.: A new two-moment bulk stratiform cloud microphysics scheme in the Community Atmosphere Model, version 3 (CAM3), part II: single-column and global results, J. Clim., 21, 3660–3679, 2008.
Gettelman, A., Liu, X., Ghan, S. J., Morrison, H., Park, S., Conley, A. J., Klein, S. A., Boyle, J., Mitchell, D. L., and Li, J.-L. F.: Global simulations of ice nucleation and ice supersaturation with an improved cloud scheme in the Community Atmosphere Model, J. Geophys. Res., 115, D18216, doi:10.1029/2009JD013797, 2010.
Gettelman, A., Liu, X., Barahona, D., Lohmann, U., and Chen, C.: Climate Impacts of Ice Nucleation, J. Geophys. Res., 117, D20201, doi:10.1029/2012JD017950, 2012.

ACPD
13, 12135–12176, 2013

Ghan, S. J. and Easter, R. C.: Impact of cloud-borne aerosol representation on aerosol direct and indirect effects, Atmos. Chem. Phys., 6, 4163–4174, doi:10.5194/acp-6-4163-2006, 2006.

Ghan, S. J. and Zaveri, R. A.: Parameterization of optical properties for hydrated internally mixed aerosol, J. Geophys. Res., 112, D10201, doi:10.1029/2006JD007927, 2007.

Ghan, S. J., Liu, X., Easter, Jr., R. C., Zaveri, R. A., Rasch, P. J., Yoon, J. H., and Eaton, B.: Toward a minimal representation of aerosols in climate models: comparative decomposition of aerosol direct, semidirect, and indirect radiative forcing, J. Clim., 25, 6461–6476. doi:10.1175/JCLI-D-11-00650.1, 2012.

Golaz, J.-C., Salzmann, M., Donner, L. J., Horowitz, L. W., Ming, Y., and Zhao, M.: Sensitivity of the aerosol indirect effect to subgrid variability in the cloud parameterization of the GFDL Atmosphere General Circulation Model AM3, J. Clim., 24, 3145–3160, 2011.

Haerter, J. O., Roeckner, E., Tomassini, L., and von Storch, J. S.: Parametric uncertainty effects on aerosol radiative forcing, Geophys. Res. Lett., 36, L15707, doi:10.1029/2009GL039050, 2009.

Hess, M., Koepke, P., and Schult, I.: Optical properties of aerosols and clouds: the software package OPAC, B. Amer. Meteor. Soc., 79, 831–844, 1998.

Hoose, C., Kristjansson, J. E., Iversen, T., Kirkevag, A., Seland, Ø., and Gettelman, A.: Constraining cloud droplet number concentration in GCMs suppresses the aerosol indirect effect, Geophys. Res. Lett., 36, L12807, doi:10.1029/2009GL038568, 2009.

Hou, Z., Huang, M., Leung, L. R., Lin, G., and Ricciuto, D. M.: Sensitivity of surface flux simulations to hydrologic parameters based on an uncertainty quantification framework applied to the Community Land Model, J. Geophys. Res., 117, D15108, doi:10.1029/2012JD017521, 2012.

Hurrell, J., M. Holland, S. Ghan, J. Lamarque, D. Lawrence, W. Lipscomb, N. Mahowald, et al.: The community earth system model: a framework for collaborative research, B. Am. Meteorol. Soc., doi:10.1175/BAMS-D-12-00121, in press, 2013.

Iacono, M. J., Mlawer, E. J., Clough, S. A., and Morcrette, J.-J.: Impact of an improved longwave radiation model, RRTM, on the energy budget and thermodynamic properties of the NCAR community climate mode, CCM3, J. Geophys. Res., 105, 14873–14890, 2000.

Jackson, C., Sen, M. K., and Stoffa, P. L.: An efficient stochastic Bayesian approach to optimal parameter and uncertainty estimation for climate model predictions, J. Climate, 17, 2828–2841, 2004.

ACPD
13, 12135–12176, 2013

Jackson, C. S., Sen, M. K., Huerta, G., Deng, Y., and Bowman, K. P.: Error reduction and convergence in climate prediction, J. Climate, 21, 6698–6709, doi:10.1175/2008jcli2112.1, 2008.

Kiehl, J. T.: Twentieth century climate model response and climate sensitivity, Geophys. Res. Lett., 34, L22710, doi:10.1029/2007GL031383, 2007.

Lamarque, J.-F., Bond, T. C., Eyring, V., Granier, C., Heil, A., Klimont, Z., Lee, D., Liousse, C., Mieville, A., Owen, B., Schultz, M. G., Shindell, D., Smith, S. J., Stehfest, E., Van Aardenne, J., Cooper, O. R., Kainuma, M., Mahowald, N., McConnell, J. R., Naik, V., Riahi, K., and van Vuuren, D. P.: Historical (1850–2000) gridded anthropogenic and biomass burning emissions of reactive gases and aerosols: methodology and application, Atmos. Chem. Phys., 10, 7017–7039, doi:10.5194/acp-10-7017-2010, 2010.

Lee, L. A., Carslaw, K. S., Pringle, K. J., and Mann, G. W.: Mapping the uncertainty in global CCN using emulation, Atmos. Chem. Phys., 12, 9739–9751, doi:10.5194/acp-12-9739-2012, 2012.

Liu, X., Penner, J. E., Ghan, S. J., and Wang, M.: Inclusion of ice microphysics in the NCAR Community Atmosphere Model version 3 (CAM3), J. Clim., 20, 4526–4547, 2007.

Liu, X., Xie, S., Boyle, J., Klein, S. A., Shi, X., Wang, Z., Lin, W., Ghan, S. J., Earle, M., Liu, P. S. K., Wang, Z., and Zelenyuk, A.: Testing cloud microphysics parameterizations in NCAR CAM5 with ISDAC and M-PACE observations, J. Geophys. Res., 116, D00T11, doi:10.1029/2011JD015889, 2011.

Liu X., Easter, Jr, R. C., Ghan, S. J., Zaveri, R. A., Rasch, P. J., Shi, X., Lamarque, J. F., Gettelman, A., Morrison, H., Vitt, F., Conley, A., Park, S., Neale, R., Hannay, C., Ekman, A. M., Hess, P., Mahowald, N., Collins, W. D., Iacono, M. J., Bretherton, C. S., Flanner, M. G., and Mitchell, D.: Toward a minimal representation of aerosols in climate models: description and evaluation in the Community Atmosphere Model CAM5, Geosci. Model Dev. 5, 709–739, doi:10.5194/gmd-5-709-2012, 2012.

Loeb, N. G., Wielicki, B. A., Doelling, D. R., Smith, G. L., Keyes, D. F., Kato, S., Manalo-Smith, N., and Wong, T.: Toward optimal closure of the earth's top-of-atmosphere radiation budget, J. Clim., 22, 748–766, 2009.

Lohmann, U. and Feichter, J.: Global indirect aerosol effects: a review, Atmos. Chem. Phys., 5, 715–737, doi:10.5194/acp-5-715-2005, 2005.

ACPD
13, 12135–12176, 2013

Lohmann, U. and Ferrachat, S.: Impact of parametric uncertainties on the present-day climate and on the anthropogenic aerosol effect, Atmos. Chem. Phys., 10, 11373–11383, doi:10.5194/acp-10-11373-2010, 2010.

Lohmann, U., Quaas, J., Kinee, S., and Feichter, J.: Different approaches for constraining global climate models of the anthropogenic indirect aerosol effect, B. Am. Meteorol. Soc., 88, 243–249, doi:10.1175/BAMS-88-2-243, 2007.

McCullagh, P. and Nelder, J. A.: Generalized Linear Models, Chapman and Hall, 1989.

Mitchell, D. L.: Parameterization of the Mie extinction and absorption coefficients for water clouds, J. Atmos. Sci., 57, 1311–1326, 2000.

Mitchell, D. L., Baran, A. J., Arnott, W. P., and Schmitt, C.: Testing and comparing the modified anomalous diffraction approximation, J. Atmos. Sci., 63, 2948–2962, 2006.

Mitchell, D. L., Rasch, P., Ivanova, D., McFarquhar, G., and Nousiainen, T.: Impact of small ice crystal assumptions on ice sedimentation rates in cirrus clouds and GCM simulations, Geophys. Res. Lett., 35, L09806, doi:10.1029/2008GL033552, 2008.

Mlawer, E. J., Taubman, S. J., Brown, P. D., Iacono, M. J., and Clough, S. A.: RRTM, a validated correlated-k model for the longwave, J. Geophys. Res., 102, 16663–16682, 1997.

Morrison, H. and Gettelman, A.: A new two-moment bulk stratiform cloud microphysics scheme in the Community Atmosphere Model, version 3 (CAM3), part I: description and numerical tests, J. Clim., 21, 3642–3659, doi:10.1175/2008JCLI2105.1, 2008.

Neale, R. B., Richter, J. H., and Jochum, M.: The impact of convection on ENSO: from a delayed oscillator to a series of events, J. Clim., 21, 5904–5924, 2008.

Park, S. and Bretherton, C. S.: The University of Washington Shallow Convection and Moist Turbulence Schemes and their impact on climate simulations with the Community Atmosphere Model, J. Clim., 22, 3449–3469, doi:10.1175/2008JCLI2557.1, 2009.

Penner, J., Quaas, J., Storelvmo, T., Takemura, T., Boucher, O., Guo, H., Kirkevåg, A., Kristjánsson, J., and Seland, Ø.: Model intercomparison of indirect aerosol effects, Atmos. Chem. Phys., 6, 3391–3405, doi:10.5194/acp-6-3391-2006, 2006.

Quaas, J., Ming, Y., Menon, S., Takemura, T., Wang, M., Penner, J. E., Gettelman, A., Lohmann, U., Bellouin, N., Boucher, O., Sayer, A. M., Thomas, G. E., McComiskey, A., Feingold, G., Hoose, C., Kristjánsson, J. E., Liu, X., Balkanski, Y., Donner, L. J., Ginoux, P. A., Stier, P., Grandey, B., Feichter, J., Sednev, I., Bauer, S. E., Koch, D., Grainger, R. G., Kirkevåg, A., Iversen, T., Seland, Ø., Easter, R., Ghan, S. J., Rasch, P. J., Morrison, H., Lamarque, J.-F., Iacono, M. J., Kinne, S., and Schulz, M.: Aerosol indirect effects – general

ACPD
13, 12135–12176, 2013

circulation model intercomparison and evaluation with satellite data, Atmos. Chem. Phys., 9, 8697–8717, doi:10.5194/acp-9-8697-2009, 2009.
Ramanathan, V. and Carmichael, G.: Global and regional climate changes due to black carbon, Nat. Geosci., 1, 221–227, 2008.
Saltelli, A. and Annonia, P.: How to avoid a perfunctory sensitivity analysis, Environ. Modell. Softw., 25, 1508–1517, 2010.
Sanderson, B. M., Piani, C., Ingram, W. J., Stone, D. A., and Allen, M. R.: Towards constraining climate sensitivity by linear analysis of feedback patterns in thousands of perturbed-physics GCM simulations, Clim. Dynam., 30, 175–190, 2008.
Schwartz, S. E.: Uncertainty requirements in radiative forcing of climate change. J. Air Waste Manage., 54, 1351–1359, 2004.
Spracklen, D. V., Jimenez, J. L., Carslaw, K. S., Worsnop, D. R., Evans, M. J., Mann, G. W., Zhang, Q., Canagaratna, M. R., Allan, J., Coe, H., McFiggans, G., Rap, A., and Forster, P.: Aerosol mass spectrometer constraint on the global secondary organic aerosol budget, Atmos. Chem. Phys., 11, 12109–12136, doi:10.5194/acp-11-12109-2011, 2011.
Tarantola, A.: Inverse Problem Theory and Methods for Model Parameter Estimation, Society of Industrial and Applied Mathematics (SIAM), Philadelphia, PA, USA, 2005.
Textor, C., Schulz, M., Guibert, S., Kinne, S., Bauer, S. E., Balkanski, Y., Berntsen, T., Berglen, T., Boucher, O., Chin, M., Dentener, F., Diehl, T., Feichter, H., Fillmore, D., Ghan, S., Ginoux, P., Gong, S., Grini, A., Hendricks, J., Horrowitz, L., Isaksen, I., Iversen, T., Kirkevag, A., Koch, D., Kristjansson, J. E., Krol, M., Lauer, A., Lamarque, J. F., Liu, X., Montanaro, V., Myhre, G., Penner, J., Pitari, G., Reddy, S., Seland, O., Stier, P., Takemura, T., and Tie, X.: Analysis and quantification of the diversities of aerosol life cycles within AeroCom, Atmos. Chem. Phys., 6, 1777–1813, doi:10.5194/acp-6-1777-2006, 2006.
Venables, W. N. and Ripley, B. D.: Modern Applied Statistics with S, Springer, 2002.
Vignati, E., Facchini, M. C., Rinaldi, M., Scannell, C., Ceburnis, D., Sciare, J., Kanakidou, M., Myriokefalitakis, S., Dentener, F., and O'Dowd, C. D.: Global scale emission and distribution of sea-spray aerosol: sea-salt and organic enrichment, Atmos. Environ., 44, 670–677, 2010.
Wang, H., Easter, R. C., Rasch, P. J., Wang, M., Liu, X., Ghan, S. J., Qian, Y., Yoon, J.-H., Ma, P.-L., and Velu, V.: Sensitivity of remote aerosol distributions to representation of cloud-aerosol interactions in a global climate model, Geosci. Model Dev. Discuss., 6, 331–378, doi:10.5194/gmdd-6-331-2013, 2013.

ACPD
13, 12135–12176, 2013

Wang, X. Q. and Sloan, I. H.: Low discrepancy sequences in high dimensions: how well are their projections distributed?, J. Comput. Appl. Math., 213, 366–386, 2008.

Yang, B., Qian, Y., Lin, G., Leung, L. R., and Zhang, Y.: Some issues in uncertainty quantification and parameter tuning: a case study of Convective Parameterization Scheme in the WRF Regional Climate Model, Atmos. Chem. Phys., 12, 2409–2427, doi:10.5194/acp-12-2409-2012, 2012.

Yang, B., Qian, Y., Lin, G., Leung, L. R., Rasch, P. J., Zhang, G. J., McFarlane, S. A., Zhao, C., Zhang, Y., Wang, H., Wang, M., and Liu, X.: Uncertainty quantification and parameter tuning in the CAM5 Zhang-McFarlane convection scheme and impact of improved convection on the global circulation and climate, J. Geophys. Res., 118, 395–415, doi:10.1029/2012JD018213, 2013.

Zhang, G. J. and McFarlane, N. A.: Sensitivity of climate simulations to the parameterization of cumulus convection in the Canadian Climate Centre general circulation model, Atmos. Ocean, 33, 407–446, 1995.

Zhao, C., Liu, X., Ruby Leung, L., and Hagos, S.: Radiative impact of mineral dust on monsoon precipitation variability over West Africa, Atmos. Chem. Phys., 11, 1879–1893, doi:10.5194/acp-11-1879-2011, 2011.

Zhao, C., Leung, L. R., Easter, R., Hand, J., and Avise, J.: Characterization of speciated aerosol direct radiative forcing over California, J. Geophys. Res. Atmos., 118, doi:10.1029/2012JD018364, 2013.

ACPD
13, 12135–12176, 2013

Table 1. CAM5 cloud microphysics and aerosol parameters of interest.

Tuning parameter	Description	Default value	Investigated range
ai	Fall speed parameter for cloud ice	700 ($m^{-1}\,s^{-1}$)	350–1400 ($m^{-1}\,s^{-1}$)
as	Fall speed parameter for snow	11.72 ($m^{0.59}\,s^{-1}$)	5.86–23.44 ($m^{0.59}\,s^{-1}$)
cdnl	Cloud droplet number limiter	0.0 (# cm^{-3})	0–1 $\times 10^{7}$ (# cm^{-3})
dcs	Auto-conversion size threshold for ice to snow	400 (μm)	100–500 (μm)
wsubmin	Minimum sub-grid vertical velocity for cloud droplet activation	0.2 ($m\,s^{-1}$)	0–1 ($m\,s^{-1}$)
sol_facti	Solubility factor for cloud-borne aerosols in stratiform clouds	1 (fraction)	0.5–1 (fraction)
sol_factic	Interstitial aerosol in convective wet removal tuning factor	0.4 (fraction)	0.2–0.8 (fraction)
refindex_dust_sw	Visible imaginary refractive index for dust	0.005 (dimensionless)	0.001–0.01 (dimensionless)
emis_DUST	Dust emission tuning factor	0.35 (dimensionless)	0.21–0.86 (dimensionless)
emis_SEAS	Sea salt emission tuning factor	1.0 (dimensionless)	0.5–2.0 (dimensionless)
emis_SOAg	SOA (g) emission scaling factor	1.5 (dimensionless)	0.5–2.0 (dimensionless)
emis_SO2	Emission tuning factor for anthropogenic SO_2	1 (dimensionless)	0–2 (dimensionless)
emis_BC	Emission tuning factor for anthropogenic BC	1 (dimensionless)	0–3 (dimensionless)
emis_POM	Emission tuning factor for anthropogenic POM	1 (dimensionless)	0–3 (dimensionless)
emis_num_a1_surf	Tuning factor of aerosol number emission in accumulation mode	1.0 (dimensionless)	0.3–5.0 (dimensionless)
emis_SO4f	Tuning factor for fraction of SO_2 emitted as sulfate	2.5 % (dimensionless)	0–5 % (dimensionless)

ACPD
13, 12135–12176, 2013

Table 2. Normalized changes of radiative fluxes due to perturbations of emission parameters in CAM5.

	Dust	Sea Salt	SOAg	SO_2	BC	POM	num_a1_surf
FNET	0.06 (0.2)	0.6 (40.7)	0.07 (0.6)	0.2 (7.3)	0.03 (0.2)	0.1 (4.5)	0.07 (2.0)
FNETC	0.05 (0.3)	0.4 (53.1)	0.1 (5.6)	0.09 (3.2)	0.05 (1.5)	0.01 (0.06)	0.01 (0.1)
LWFNETC	0.07 (25.6)	0.02 (8.3)	0.01 (1.4)	0.02 (6.3)	0.01 (2.8)	0.02 (10.4)	0.01 (3.5)
SWFNETC	0.1 (1.4)	0.5 (50.6)	0.2 (5.6)	0.1 (3.9)	0.06 (1.8)	0.03 (0.4)	0.003 (0.01)
CF	0.06 (0.7)	0.1 (6.8)	0.07 (2.0)	0.1 (6.6)	0.04 (0.98)	0.1 (11.2)	0.08 (7.8)
LWCF	0.06 (1.4)	0.05 (2.0)	0.03 (0.6)	0.1 (20.8)	0.03 (2.0)	0.06 (7.9)	0.04 (5.1)
SWCF	0.06 (0.6)	0.1 (4.2)	0.06 (1.7)	0.3 (34.4)	0.01 (0.1)	0.06 (3.4)	0.04 (2.4)

[1] The normalized variation of radiative fluxes is calculated through dividing parameter-induced variation of radiative fluxes by the scale range of emission change. Therefore, the unit is W m^{-2}/(unit scale change).

[2] The values in parenthesis are the relative contributions (%) of parameter-perturbations to the total variance of FNET resulting from perturbation of emission parameters.

ACPD
13, 12135–12176, 2013

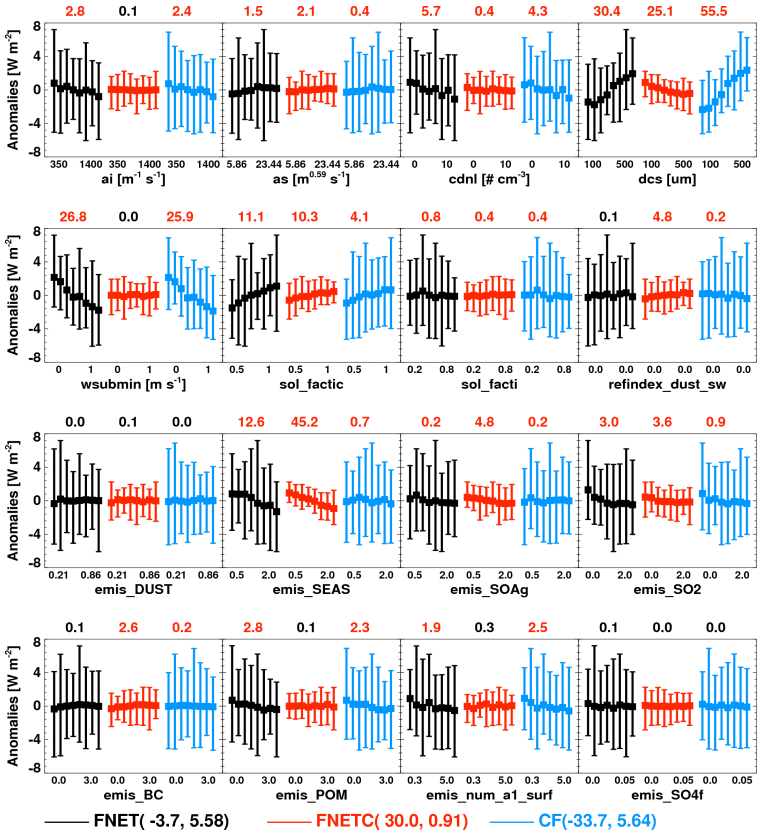

Fig. 1. Anomalies of variation of global mean FNET, clear-sky FNET (FNETC), and net (SW + LW) cloud forcing at TOA (CF) in response to the perturbations of 16 parameters from the 256 CAM5 simulations. The 256-simulation mean and variance are shown, respectively, in the parenthesis for FNET, FNETC, and CF. The numbers above each plot box represent the relative contribution (percentage) of each input parameter perturbation to the overall FNET, FNETC, and CF variations. Red means the contribution with 95 % statistic significance.

ACPD
13, 12135–12176, 2013

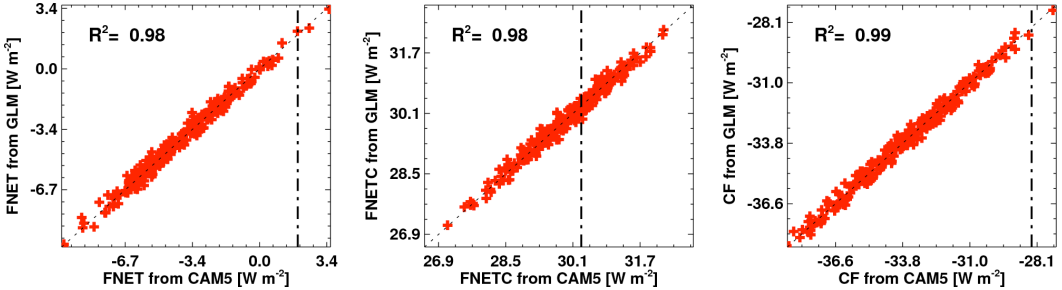

Fig. 2. GLM-fitted response variables versus the CAM5 simulations for FNET, FNETC, and CF. The black dash lines represent the values simulated by CAM5 with default parameters.

ACPD
13, 12135–12176, 2013

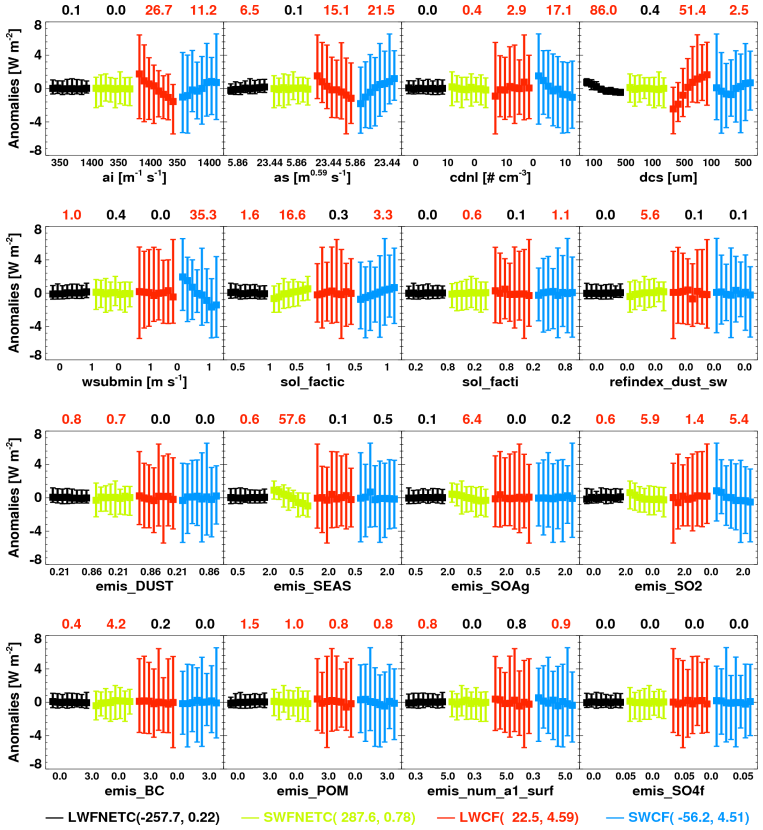

Fig. 3. Same as Fig. 1, but for anomalies of variation of global mean LW FNETC, SW FNETC, LWCF, and SWCF in response to the perturbations of 16 parameters from the 256 CAM5 simulations.

ACPD
13, 12135–12176, 2013

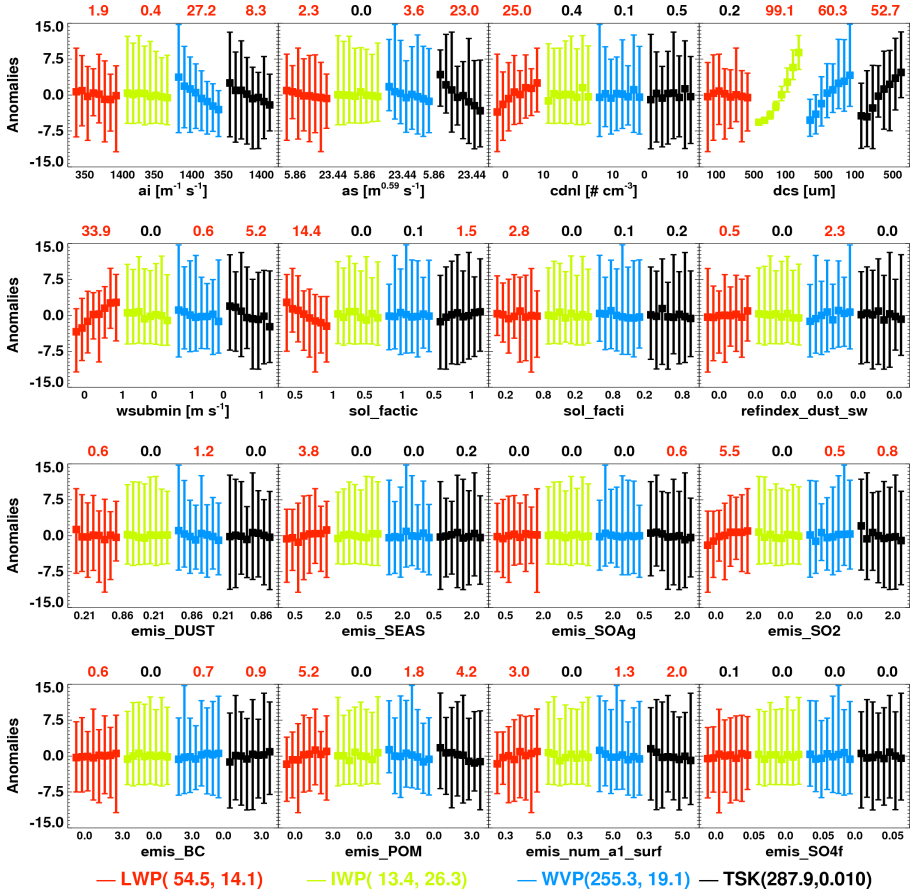

Fig. 4. Same as Fig. 1, but for anomalies of variation of global mean liquid water path (LWP), ice water path (IWP), water vapor path (WVP), and surface temperature (TSK) in response to the perturbations of 16 parameters from the 256 CAM5 simulations. The units for anomalies of LWP, IWP, WVP, and TSK are $g\,m^{-2}$, $g\,m^{-2}$, $hg\,m^{-2}$, and $K\,50^{-1}$, respectively.

ACPD
13, 12135–12176, 2013

A sensitivity study of radiative fluxes

C. Zhao et al.

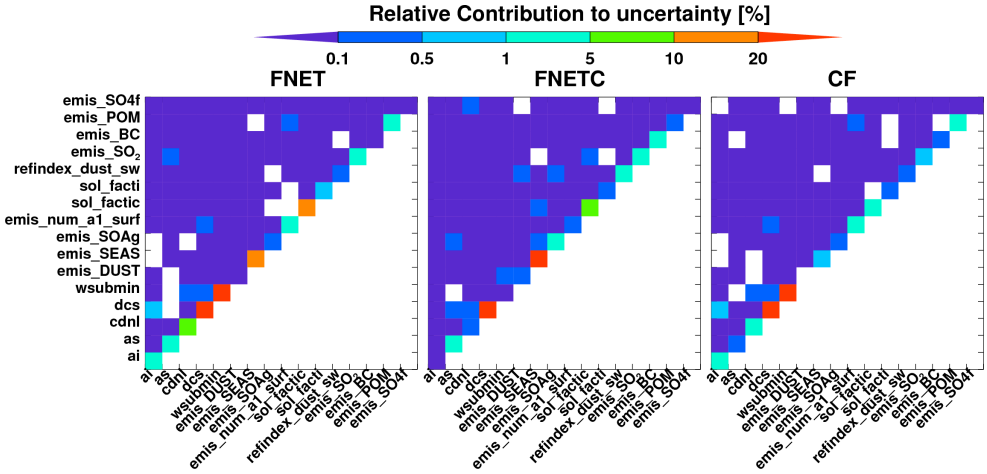

Fig. 5. Relative contributions (percentage) of perturbations of individual parameter and their interactions to the variations of FNET, FNETC, and CF estimated by the GLM.

ACPD
13, 12135–12176, 2013

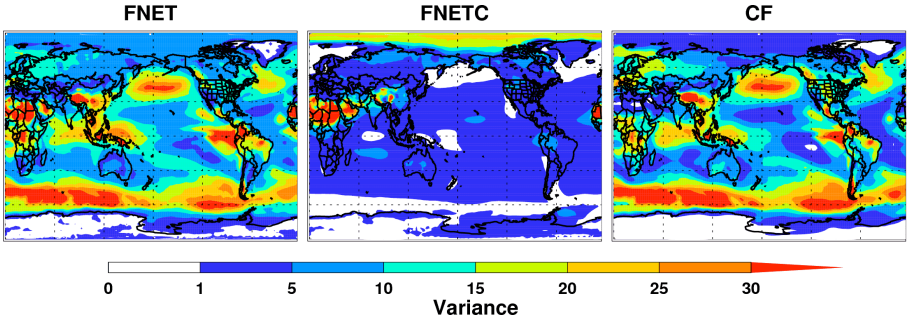

Fig. 6. Global spatial distribution of variance of FNET, FNETC, and CF (unit in $W^2\,m^{-4}$) in response to the perturbations of 16 parameters from the 256 CAM5 simulations.

ACPD
13, 12135–12176, 2013

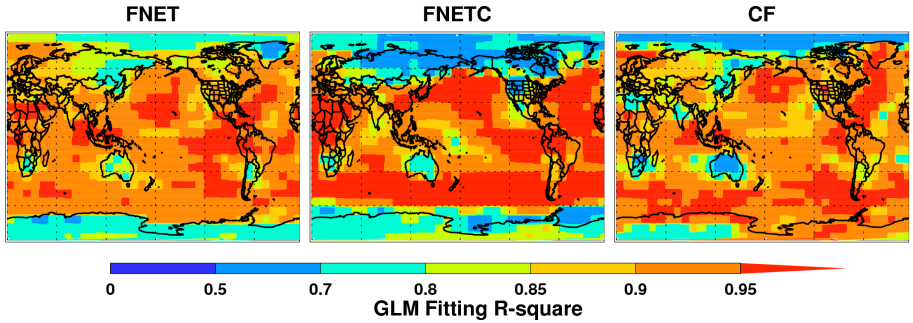

Fig. 7. Spatial distributions of *R* square of the GLM models for FNET, FNETC, and CF.

ACPD
13, 12135–12176, 2013

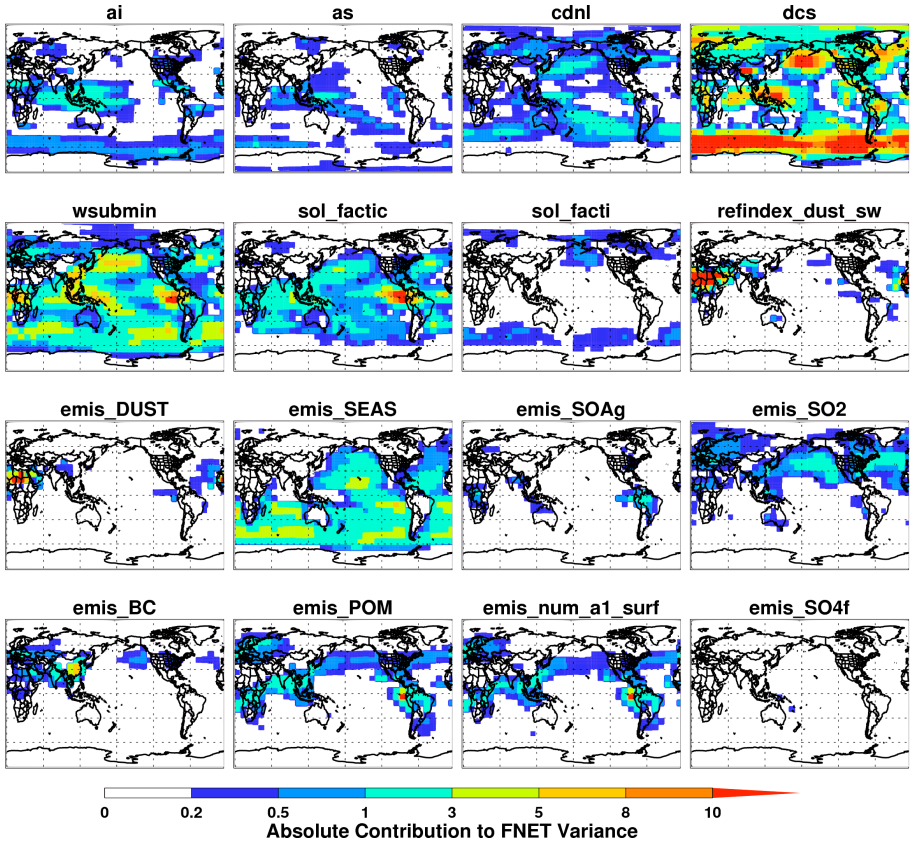

Fig. 8. Global spatial distribution of absolute FNET variance (unit in $W^2\,m^{-4}$) in response to the perturbation of each of the 16 input parameters predicted by the GLM.

ACPD
13, 12135–12176, 2013

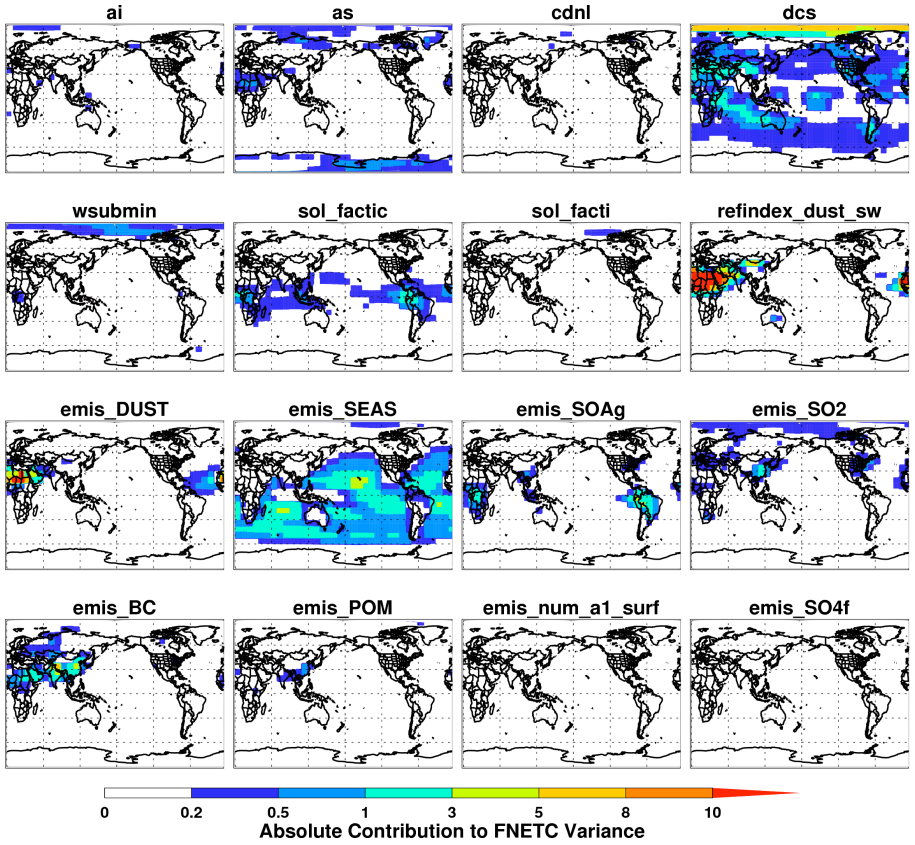

Fig. 9. Global spatial distribution of absolute FNETC variance (unit in $W^2\,m^{-4}$) in response to the perturbation of each of the 16 input parameters predicted by the GLM.

ACPD
13, 12135–12176, 2013

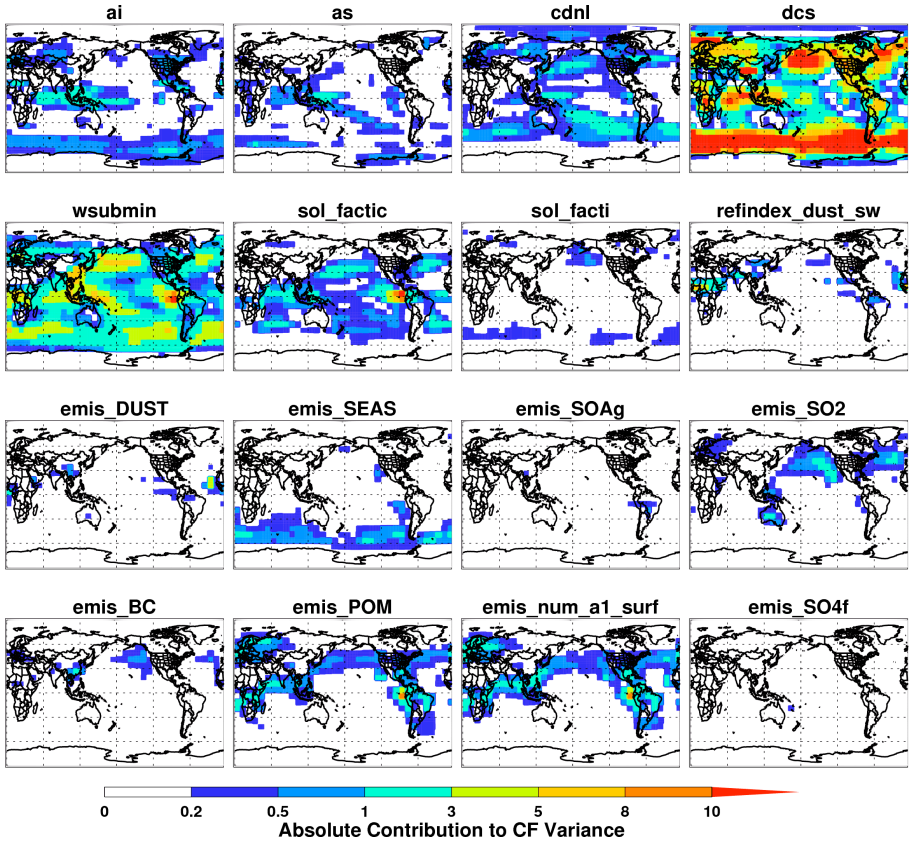

Fig. 10. Global spatial distribution of absolute CF variance (unit in $W^2\,m^{-4}$) in response to the perturbation of each of the 16 input parameters predicted by the GLM.

ACPD
13, 12135–12176, 2013

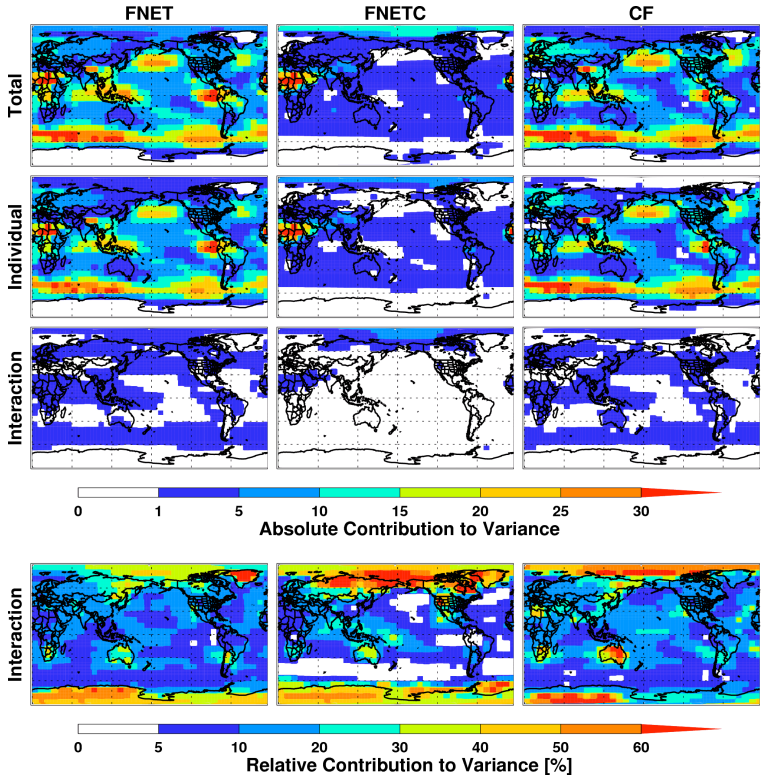

Fig. 11. Global spatial distribution of absolute variance of FNET, FNETC, and CF (unit in $W^2 m^{-4}$) in response to the total, main, and interaction effects of perturbations of 16 input parameters predicted by the GLM, the percentage of variance of FNET, FNETC, and CF in response to the interaction effect.

ACPD
13, 12135–12176, 2013